Novel variants of unknown significance cause pathogenesis through distinct mechanisms in spinocerebellar ataxia 14

Robin Kalsbeek

Research Project II

Oct. 2021 – Mar. 2022

Supervised by prof. Dineke S. Verbeek, PhD

Biomedical Sciences – Biology of Aging Research

University of Groningen

Abstract

Spinocerebellar ataxia type 14 (SCA14) is a dominantly inherited ataxia caused by missense mutations in the *PRKCG* gene encoding protein kinase c-gamma (PKCγ). Patients with SCA14 suffer from a slowly progressing cerebellar ataxia. Most pathogenic mutations are found in the C1 domain of PKCγ and cause pathogenesis through increased activity, mislocalization, and protein aggregation. In many cases, genetic tests reveal variants of unknown significance in patients (VUSes). Because SCA14 is a late-onset disease with low prevalence, segregation studies are not always possible, leaving these VUSes unclassified and the patients without a diagnosis. In the present study, we provide evidence on the pathogenicity of the PKCγ variants H174P and R239W in the C2 domain. We performed functional studies on these variants with overexpression plasmids encoding the cDNA of these variants, and we used the novel CRISPR/Cas9 technique prime editing to make isogenic cell models in the human neuroblastoma cell line SH-SY5Y. We showed that both PKCγ H174P and R239W cause pathogenesis through distinct mechanisms. Both PKCγ H174P and R239W form aggregates, PKCγ R239W inhibits proteasomal degradation, and PKCγ H174P increases the activity of PKCγ. Furthermore, Ca^{++} signaling was sufficient to activate PKCγ H174P, and its expression was toxic in SH-SY5Y cells.

Table of Contents

Introduction

Spinocerebellar ataxias (SCAs) are a group of dominantly inherited ataxias characterized by degeneration of the cerebellum and sometimes the spinal cord (Soong & Paulson, 2007). The most common types of SCA are caused by CAG repeat expansions in various genes. Other types of SCA are caused by different genetic patterns (Carlson et al., 2009). SCA14 is an autosomal dominant type of ataxia, caused by mostly missense mutations in the *PRKCG* gene encoding protein kinase c-gamma (PKCγ), leading to cerebellar atrophy and late-onset Purkinje cell degeneration (Seki et al., 2005). This neurodegeneration causes SCA14 patients to suffer from a slowly progressing cerebellar ataxia (Chen et al., 2003).

PKCγ is a serine/threonine protein kinase specifically expressed in brain tissue. It is required for neuronal differentiation to Purkinje cells, in which it regulates dendritic growth and Ca^{++} permeability (Shimobayashi & Kapfhammer, 2017). Like other classical PKCs (α, βI, and βII), PKCγ is phosphorylated by PDK-1 and by autophosphorylation, and can then bind Ca^{++}, upon which it translocates to the plasma membrane. At the plasma membrane, PKCγ binds diacylglycerol (DAG), upon which its conformation changes, revealing the kinase domain. It can then act as a second messenger downstream of phospholipase C (PLC), phosphorylating serine and threonine residues on its various substrates. (Newton, 2010)

Since SCA14 is an autosomal dominant disease, it is thought to be caused by a gain of function of PKCγ through either increased activity, mislocalization, or formation of aggregates (Shimobayashi & Kapfhammer, 2021; Wong et al., 2018). Many missense mutations have been found in the C1 domain, which is the DAG-binding domain (Schmitz-Hübsch et al., 2021). These missense mutations in the C1 domain often destabilize the protein structure, causing it to misfold and aggregate (Jezierska et al., 2014; Seki et al., 2005; Wong et al., 2018). Some of these mutations also affected the phosphorylation status of PKCγ, thereby impairing proteasomal degradation and inducing ER stress (Jezierska et al., 2014; Seki et al., 2007).

With the current guidelines (Ellard et al., 2020), it is challenging to perform genetic tests for SCA14, as there is no established model of pathogenicity and because, in many cases, new genetic variants of unknown significance (VUSes) are found (Schmitz-Hübsch et al., 2021). Because SCA14 is a late-onset disease with low prevalence, segregation studies are often difficult to perform, leaving these VUSes unclassified. The guidelines for Variant Classification of the American College of Medical Genetics state that a VUS is not sufficient to justify a clinical diagnosis (Ellard et al., 2020). As such, this often leaves the patient without a diagnosis.

Two examples of such VUSes in SCA14 are H174P and R239W, in the C2 domain of PKCγ, which binds Ca^{++}. The H174P variant was first reported in an isolated case of late-onset ataxia, which could not be explained by mutations in genes for SCA1, 2, 3, 6, 7, 12, 17, and FRDA (van Gaalen et al., 2013). However, familial segregation studies showed that the H174P variant occurred as a *de novo* mutation. As such, it was concluded that the H174P variant is a pathogenic mutation causal to the disease without performing functional analyses.

The R239W variant was recently reported in a case of late-onset ataxia (Ghorbani et al., 2022). Routine testing for mutations in the genes for SCA1, 2, 3, 6, 7, and 17 left the patient without a diagnosis. Segregation studies on the R239W variant could not be performed because the patient's family members were unreachable. Since this was the first case in which the R239W variant had presented itself, and C2 domain mutations are not prevalent, there was not enough evidence to conclude that the variant was causal to the disease.

To reclassify these VUSes as benign or pathogenic, follow-up studies need to be done. Protein modeling can predict the effect of the variant on the conformation of the protein and its interaction with other biomolecules. Therefore, protein modeling is a helpful tool to initially prioritize VUSes for functional studies since these can be very time-consuming (Ghorbani et al., 2022).

Until now, functional studies in cells were often done using overexpression of the protein variants. Overexpression screens are relatively easy to perform and offer many new insights, especially on gain-of-function mechanisms. However, overexpression inherently causes a loss of protein stoichiometry, which leads to an overexpression phenotype skewing the results (Prelich, 2012).

The advent of CRISPR/Cas9 genome editing techniques has made it accessible to create isogenic cell and animal models more representative of the disease (Deneault et al., 2021). Traditionally, genome editing with CRISPR/Cas9 was done by creating a double-strand break (DSB) and providing a homology-directed repair (HDR) template to be recombined, introducing the variant of interest. Although this technique is highly versatile, it has the drawback of introducing off-target mutations and insertion-deletion mutations (indels; Deneault et al., 2021).

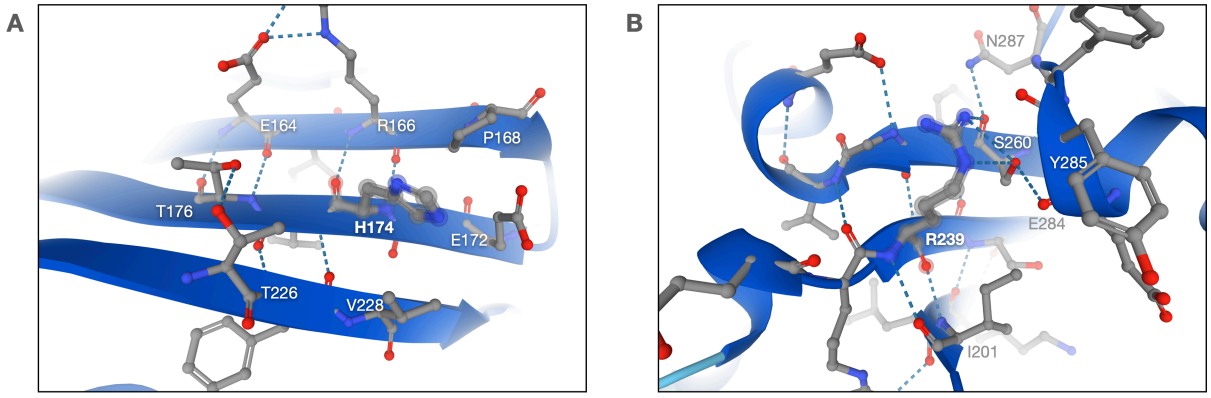

Figure 1. Ball-and-stick model of WT PKCγ, with cylinders and spheres for bonds and atoms, dotted lines for hydrogen bonds, and ribbons representing the backbone (Jumper et al., 2021). (A) Section of PKCγ focused on H174. (B) Section of PKCγ focused on R239.

A recent publication described the development of the prime editing technique, a novel approach to Cas9-based genome editing without DSBs or HDR templates (Anzalone et al., 2019). Instead, the prime editing technique uses a nicking Cas9 endonuclease fused to an M-MLV reverse transcriptase. This prime editor enzyme is guided by a prime editing guide RNA (pegRNA) that contains the spacer region guiding the nicking Cas9 to the target DNA, a reverse transcriptase (RT) template containing the edit, and a primer binding site. The primer binding site hybridizes with the nicked target DNA, and the RT template is reverse transcribed, introducing the intended edit. The authors showed that this mechanism significantly reduced the probability of introducing off-target mutations and indels compared to the conventional CRISPR/Cas9 technique (Anzalone et al., 2019).

In the present study, we aim to provide evidence on the pathogenicity of the PKCγ variants H174P and R239W. To this end, we performed functional studies using overexpression plasmids encoding these protein variants in 293T cells. Additionally, we performed the prime editing technique to make an isogenic cell model in the human neuroblastoma cell line SH-SY5Y for functional studies more representative of the disease. We will study whether the novel prime editing technique is a viable alternative to more traditional CRISPR/Cas9 techniques to screen for VUSes. A structural model of PKCγ shows that H174 is part of a β-sheet in the highly conserved C2 domain (Fig. 1a). The H174P substitution will likely cause a bend or a bulge in this β-sheet since proline has a distinct ϕ-angle that is not compatible with the standard β-sheet structure, therefore changing the secondary structure of the protein (Li et al., 1996). R239 interacts with S260 on the β-sheet next to it (Fig. 1b), which likely contributes to stabilizing the C2 domain structure. The R239W variant substitutes the positively charged arginine residue for a hydrophobic tryptophan in this position, thereby losing the electrostatic interaction with S260. As such, we hypothesize that the H174P and R239W variants destabilize the native conformation of the C2 domain and will affect the ability of PKCγ to bind Ca^{++}, increasing biological activity through the loss of inhibition.

Methods

Cell culture and transient transfection

Cells were cultured to confluency up to acceptable passage number and regularly checked for mycoplasma. Human embryonic kidney (HEK) 293T cells (ATCC) were cultured in DMEM + 10% FBS + 100 U/ml penicillin + 100 µg/ml streptomycin (Gibco). SH-SY5Y cells (ATCC) were cultured in DMEM + 15% FBS + 100 U/ml penicillin + 100 µg/ml streptomycin (Gibco). 293T cells were transiently transfected with polyethyleneimine (Polysciences) according to the manufacturer's protocol and cultured 48h post-transfection. SH-SY5Y cells were transiently transfected by electroporation with a 4D-Nucleofector System and SF Cell Line 4D-Nucleofector X kit (Lonza) according to the manufacturer's protocol.

Solutions and chemicals

Biochemicals were diluted in pre-warmed growth medium prior to adding to the cells. Cycloheximide (Sigma C4859) was used at a final concentration of 50 µg/ml. MG-132 from a 10 mM stock was diluted to a final concentration of 10 µM. A23187 (Sigma C7522) was used at 2 µM (Sigma). TPA (Sigma P1585) was used at 20 nM.

Plasmid cloning and mutagenesis PCR

For the PKCγ overexpression experiments, we used previously described constructs for wildtype PKCγ-EGFP and PKCγ R239W-EGFP (Ghorbani et al., 2022; Verbeek et al., 2008). The H174P variant was introduced in WT PKCγ-EGFP using the QuickChange II XL Site-Directed Mutagenesis Kit (Agilent Technologies) using specific primers (Supplementary Table 1), and verified by Sanger sequencing.

For the prime editing experiment, we used the previously described constructs pCMV-PE2-P2A-GFP (Addgene #132776), pU6-pegRNA-GG-acceptor (Addgene #132777), and pBPK1520 (Addgene #65777; Anzalone et al., 2019). The pegRNA and sgRNA-PE3B sequences were designed using pegFinder (Chow & Chen, 2020; Kim et al., 2021). The pegRNA inserts were created by hybridizing single-stranded oligonucleotides (Supplementary Table 1) and cloned into the pU6-pegRNA-GG-acceptor vector through Golden Gate assembly with Eco31I FastDigest endonuclease and T7 ligase (Thermo Scientific). The sgRNA-PKCg-R239W-PE3B insert was created by hybridizing single-stranded oligonucleotides (Supplementary Table 1) and cloned into the pBPK1520 vector through Golden Gate assembly with Esp3I FastDigest endonuclease and T7 ligase (Thermo Scientific).

Prime editing

SH-SY5Y cells were transiently transfected by electroporation as described before with pCMV-PE2-P2A-GFP, pU6-pegRNA-GG-acceptor, and pBPK1520-sgRNA-PE3B plasmids, and cultured for 6 days.

Subsequently, cells were dissociated with 0.05% trypsin-EDTA and resuspended in DMEM. Cell suspensions were filtered through a 35-µm nylon cell strainer (Corning Life Sciences) and stained with 4 µg/ml propidium iodide (Roche). Flow cytometry was performed on a Sony SH-800S with equipped with a 100 µm microfluidic sorting chip, at the UMCG Flow Cytometry Unit (Groningen, the Netherlands). Fluorescence-activated cell sorting (FACS) was performed, selecting for a GFP-positive and PI-negative population and sorting single cells into 96-well culture plates. Cells were cultured up to confluency and subcloned for genome isolation using QuickExtract (Lucigen).

From the extracted genomic DNA, the region of interest was amplified by PCR with AmpliTaq Gold Fast PCR (Applied Biosystems) and an initial screening was done by endonuclease restriction to detect the presence of an edit. Introduction of the R239W edit would introduce a restriction site for the AfeI endonuclease (NEB). Introduction of the H174P edit would remove a restriction site for the BstXI endonuclease (NEB). After initial screening, the genomic edit was confirmed by performing Sanger sequencing on the PCR fragment.

SH-SY5Y differentiation

SH-SY5Y cells were seeded to 50% confluency on 10 cm cell culture plates (Corning). Upon reaching 80% confluency, cells were washed twice with PBS to remove residual serum and media was changed to Neurobasal medium + GlutaMAX + B27 (Gibco), supplemented with 10 µM ATRA (Sigma). This media was replaced every 48h for 5 days and cells were kept in the dark. Subsequently, media was refreshed to Neurobasal medium + GlutaMAX + B27, supplemented with 50 ng/ml BDNF (Sigma P3795) and refreshed 50:50 every 72h for 12 days.

Immunofluorescence

Cells were grown on coverslips, fixated in 4% formaldehyde in PBS for 15 mins and permeabilized in 0.01% Triton X-100 in PBS 5 mins. Coverslips were blocked in PBS+ (0.5% BSA, 0.15% glycine in PBS) for 2 hours and incubated with primary antibodies (Supplementary Table 2) overnight at 4ºC. After washing with PBS+, coverslips were incubated with Cy3-conjugated secondary antibodies (Supplementary Table 2) for 90 mins at RT and mounted with DAPI-containing mountant solution (Vectashield, Vector Laboratories) before imaging.

Fluorescent microscopy

Live cells were imaged with an Evos FL (Invitrogen) digital inverted fluorescence microscope equipped with 10X Fl and 20X Fl objectives. Fixated cells were imaged with a Zeiss Axio Observer Z1 digital inverted fluorescence microscope equipped with a Plan-Apochromat 40x/1.3 Oil DIC objective and an AxioCam MRm camera. Micrographs were captured using ZEN pro (Zeiss) software. Micrographs were processed and analyzed with Fiji [Schindelin2012]. Cell confluency was quantified by applying a threshold on brightfield micrographs to remove the background and measuring the area fraction of non-zero pixels.

Immunoblotting

Cells were washed once with ice-cold PBS and lysed in ice-cold FTA lysis buffer + 2% SDS + 1% phosphatase inhibitor cocktail 3 (P0044, Sigma) on ice. Lysates were centrifuged at 12,000x g and sonicated 2x 5 seconds. Protein concentrations were normalized using the Pierce BCA protein assay (Thermo Fisher Scientific). Dilute lysates were precipitated in 20% (w/v) trichloroacetic acid (TCA) for 10 mins at 4ºC and centrifuged 5 mins at 14,000x g. Pellets were washed twice in ice-cold 100% acetone and dried at 95ºC for 5 mins. Normalized lysates and TCA precipitated pellets were taken up in 4x Laemmli buffer containing 10% β-mercaptoethanol and heated at 95 ºC for 5 mins before loading equal amounts on 10% SDS-PAA gels.

SDS-PAGE was performed in Tris-glycine buffer + 1% SDS at 30 mA per gel. Proteins were transferred to PVDF membrane (Amersham Hybond P, 0.45 µm pore size) in Towbin buffer + 20% methanol overnight at 30V, 4ºC using a wet-transfer setup. Transfer efficiency was assessed by Ponceau S staining before blocking in 5% (w/v) milk powder (Campina) in TBS-T for 1 hour at RT. Membranes were incubated with primary antibodies (Supplementary Table 2) overnight at 4ºC and with HRP-conjugated secondary antibodies (Supplementary Table 2) for 1 hour at RT. Proteins were visualized with ECL (0.1 M Tris HCl pH 8.5, 200 µM p-coumaric acid (Sigma), 1.25 mM luminol (Sigma), 0.045% hydrogen peroxide) and chemiluminescence was detected with a Bio-Rad ChemiDoc MP. Protein amounts were calculated using densitometry (Image Lab, Bio-Rad).

Phosphorylation of PKC substrates was assessed by performing immunoblotting against P-Ser of PKC substrates, and the range of 25-130 kDa was quantified by densitometry. Relative phosphorylation was calculated by normalizing phosphorylated PKC substrates to tubulin, and standardized to EGFP-transfected controls.

Results

In order to study the change in characteristics of PKCγ caused by the missense variants R239W and H174P, we followed two different approaches. First, we made use of expression plasmids encoding these protein variants, and transiently expressed these in HEK293T cells for functional studies. Second, we used prime editing to introduce these variants in an isogenic model of SH-SY5Y cells.

Overexpression studies

Expression plasmids with the full-length cDNA encoding wildtype PKCγ and PKCγ R239W, both C-terminally tagged with enhanced green fluorescent protein (EGFP), were already available (Ghorbani et al., 2022; Verbeek et al., 2008). The presence of the fluorescent tag EGFP facilitated fluorescent microscopy and immunoblotting assays and did not impair kinase activity (Verbeek et al., 2008). To also be able to study the change in characteristics of PKCγ caused by the H174P variant, we introduced this variant in the cDNA of PKCγ by performing mutagenesis PCR on the WT PKCγ-EGFP plasmid as described in the Methods section.

PKCγ R239W and H174P mislocalize and condensate

Previous studies have shown that WT PKCγ-EGFP is a conformationally stable protein that is diffusely localized to the cytosol (Jezierska et al., 2014; Seki et al., 2005). However, changes in protein stability and protein solubility leading to the formation of foci have been reported for various pathogenic PKCγ mutations in the past (Jezierska et al., 2014; Seki et al., 2005).

To study if the R239W and H174P variants cause changes in protein expression, stability, and localization, we transiently expressed WT PKCγ-EGFP, PKCγ R239W-EGFP and PKCγ H174P-EGFP for 48h in HEK293T cells. Using fluorescent microscopy, we confirmed that WT PKCγ-EGFP is a soluble protein that localizes to the cytosol (Fig. 2). PKCγ R239W-EGFP is mostly a soluble protein, although we observed dot-like foci in 1.3% of the cells and massive foci in 5.1% of the cells (Fig. 3a, 3b). Similarly, for

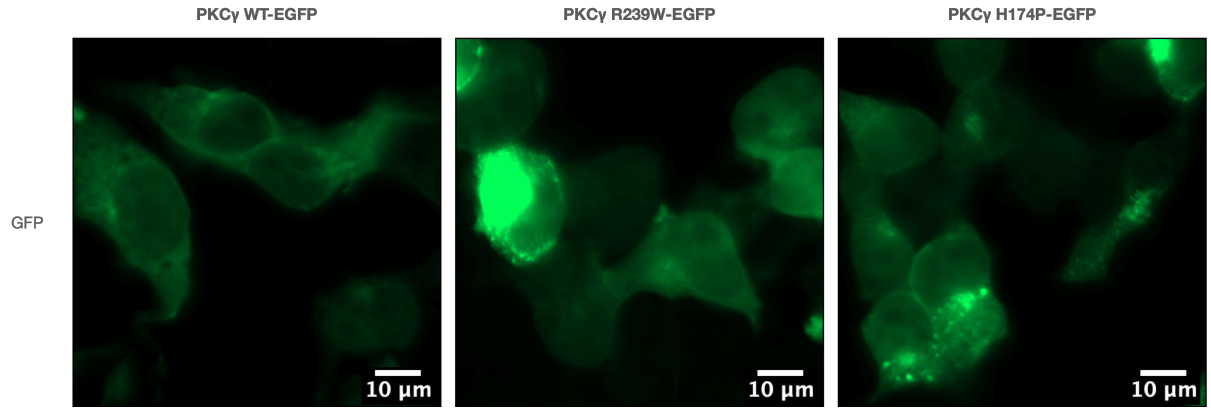

Figure 2. Widefield fluorescent micrographs of HEK293T cells expressing WT PKCγ-EGFP and PKCγ R239W-EGFP for 48h. Representative images shown. Scale bar denotes 10 µm.

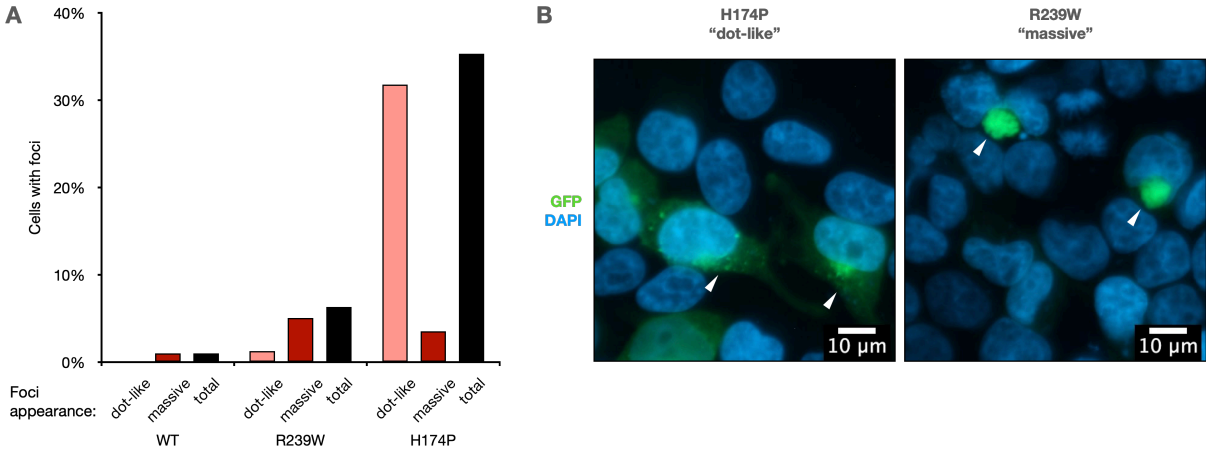

Figure 3. WT PKCγ-EGFP, PKCγ R239W-EGFP, and PKCγ H174P-EGFP were expressed for 48h in HEK293T cells before fixating and mounting. (A) Percentage of expressing cells with foci, categorized as dot-like and massive (n = 300). (B) Widefield fluorescent micrographs of PKCγ H174P-EGFP expressing cells with dot-like foci (arrows), and PKCγ R239W-EGFP expressing cells with massive foci (arrows). Representative images shown. Scale bar denotes 10 µm.

PKCγ H174P-EGFP, we observed the foci formation, albeit more often and with a different appearance. We found dot-like foci in 31.8% of the cells and massive foci in 3.5% of cells expressing PKCγ H174P-EGFP (Fig. 3a, 3b). These foci were almost not seen in cells expressing WT PKCγ-EGFP. (Fig. 2, 3a)

R239W and H174P variants affect PKCγ abundance

Next, we sought to study the difference in PKCγ-EGFP abundance between WT and the two variants by measuring the relative protein abundance via immunoblotting and densitometry. At first, we performed immunoblotting using a monoclonal antibody raised against PKCγ and one against actin as a loading control. Interestingly, we found that PKCγ R239W-EGFP is 3.0x less abundant than WT PKCγ-EGFP

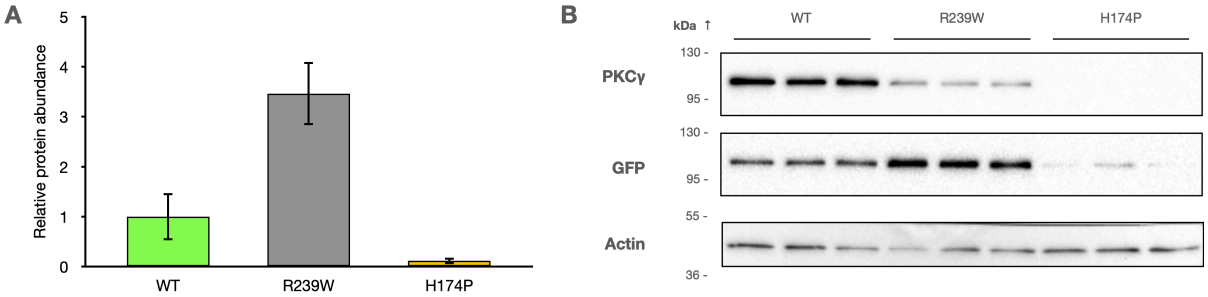

Figure 4. (A) Relative protein abundance of WT PKCγ-EGFP, PKCγ R239W-EGFP, and PKCγ H174P-EGFP at steady-state, quantified as GFP normalized to actin. Bars represent mean ± standard deviation (n = 3).
(B) Immunoblot of WT PKCγ-EGFP, PKCγ R239W-EGFP, and PKCγ H174P-EGFP. Lysates from transiently transfected HEK293T cells were run on 10% gels under denaturing conditions. After transfer to PVDF membrane the blotted bands were immunodetected with specific antibodies against PKCγ, GFP, and actin and subsequently visualized with peroxidase labeled secondary antibodies.

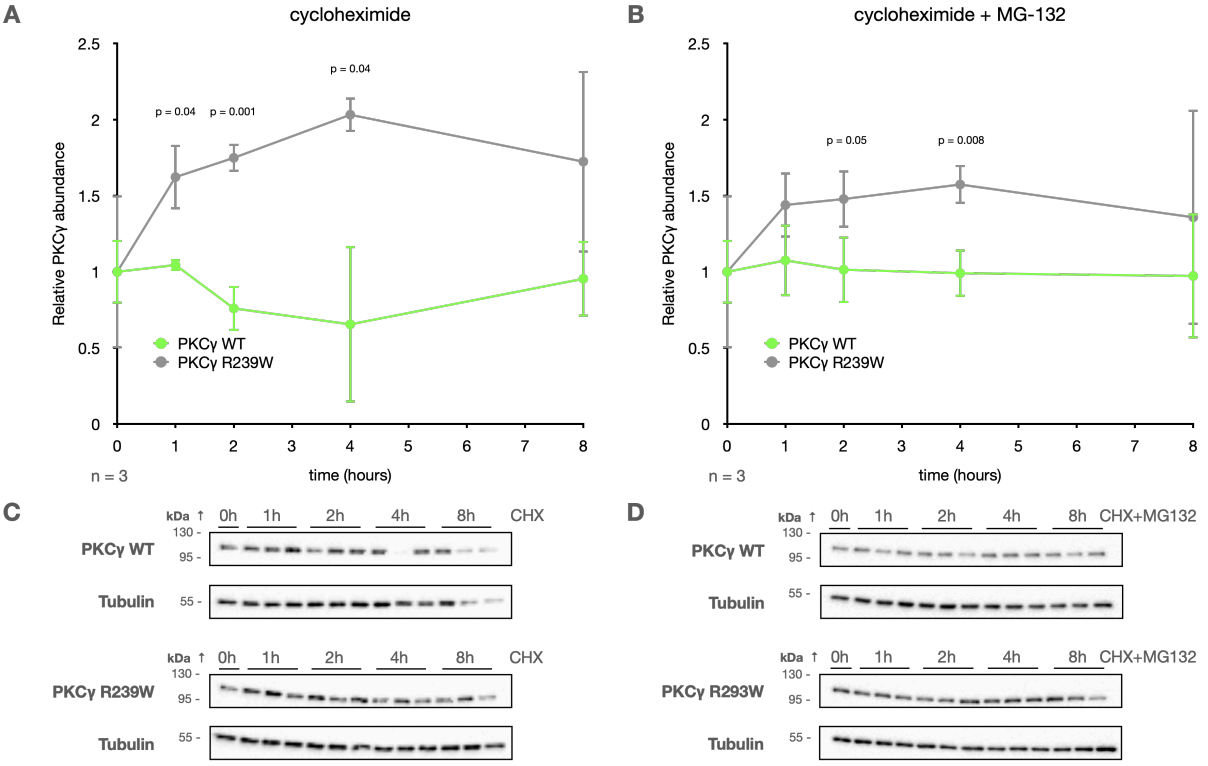

Figure 5. (A) Fold change in protein abundance of WT PKCγ-EGFP and PKCγ R239W-EGFP upon treatment with 50 µg/ml cycloheximide for 0, 1, 2, 4, and 8 hours, quantified as GFP normalized to tubulin. Graphs represent mean ± standard deviation (n = 3). Significant differences (unpaired Student *t*-test, two-tailed) are indicated with their p-values.
(B) Fold change in protein abundance of WT PKCγ-EGFP and PKCγ R239W-EGFP upon treatment with 50 µg/ml cycloheximide and 10µM MG-132 for 0, 1, 2, 4, and 8 hours, quantified as GFP normalized to tubulin. Graphs represent mean ± standard deviation (n = 3).
(C) Immunoblot of WT PKCγ-EGFP and PKCγ R239W-EGFP expressing cells upon treatment with 50 µg/ml cycloheximide for 0, 1, 2, 4, and 8 hours.
(D) Immunoblot of WT PKCγ-EGFP and PKCγ R239W-EGFP expressing cells upon treatment with 50 µg/ml cycloheximide and 10 µM MG-132 for 0, 1, 2, 4, and 8 hours. Lysates from transiently transfected HEK293T cells were run on 10% gels under denaturing conditions. After transfer to PVDF membrane the blotted bands were immunodetected with specific antibodies against GFP and tubulin, and subsequently visualized with peroxidase labeled secondary antibodies.

(Fig. 4b). Furthermore, we could not detect any PKCγ H174P-EGFP with this antibody, although PKCγ H174P-EGFP was observed using fluorescent microscopy (Fig. 2).

Therefore, we next immunoblotted with a monoclonal antibody raised against EGFP (anti-living colors). From this, the results were more in line with our estimations based on microscopy. We now found that PKCγ R239W-EGFP was 3.5x more abundant than PKCγ WT-EGFP, and could detect PKCγ H174P-EGFP (Fig. 4b). This protein variant was 8.7x less abundant than PKCγ WT-EGFP (Fig. 4a, 4b), in line with our estimations based on microscopy.

PKCγ R239W is maintained at a higher level than WT PKCγ

To study if changes to the half-life of PKCγ caused the increased abundance of the R239W variant, we transiently expressed both GFP-tagged proteins in HEK293T cells for 48h and treated cells with 50 µg/ml cycloheximide (Sigma) for up to 8 hours to inhibit protein synthesis. Cells were harvested and lysed at 0, 1, 2, 4, and 8 hours after treatment, and immunoblot analysis was performed against EGFP and tubulin to study the kinetics of PKCγ-EGFP degradation.

As shown in Figures 5a and 5c, we detected no degradation of PKCγ R239W-EGFP during 8 hours of treatment with cycloheximide, which shows that it is a very long-lived protein. Contrastingly, after 2 hours of treatment with cycloheximide, a significant portion of WT PKCγ-EGFP is already degraded and there is a clear trend of WT PKCγ-EGFP being continually degraded (Fig. 5a, 5c).

R239W impairs proteasomal degradation of PKCγ

To investigate whether the degradation of WT PKCγ-EGFP occurs through the ubiquitin-proteasome system (UPS), overexpressing cells were also subjected to a combination of 50 µg/ml cycloheximide and 10 µM proteasome inhibitor MG-132 (Lee & Goldberg, 1996). As can be seen in the graphs in Figures 5b and 5d, the addition of MG-132 inhibited protein degradation of WT PKCγ-EGFP.

Since we did not observe any degradation of PKCγ R239W-EGFP after blocking protein synthesis, which is mediated by UPS as was shown for WT PKCγ-EGFP, we next investigated if PKCγ R239W-EGFP and WT PKCγ-EGFP are differentially targeted for proteasomal degradation. To this end, we transiently expressed WT PKCγ-EGFP and PKCγ R239W-EGFP for 48h in HEK293T cells and performed immunofluorescence against endogenous ubiquitin which is conjugated to proteins targeted for degradation. As a positive control, cells were also treated with 10 µM proteasome inhibitor MG-132 for 18h before fixating. For cells expressing WT PKCγ-EGFP (without MG-132), we observed diffuse background levels of ubiquitin that did not colocalize with PKCγ (Fig. 6a). Moreover, we did not observe an increase in ubiquitin in cells expressing WT PKCγ-EGFP over non-expressing cells (Fig. 6b). In cells treated with proteasome inhibitor MG-132, we observed that ubiquitin intensity had increased overall and was present in foci. However, we did not find a correlation between either increased ubiquitin or ubiquitin foci and WT PKCγ-EGFP expression.

Contrastingly, we observed a higher intensity of ubiquitin in cells expressing PKCγ R239W-EGFP compared to non-expressing cells (Fig. 6a). Upon treatment with MG-132, we observed an overall increase in ubiquitin and ubiquitin in foci, but this increase did not correlate with PKCγ R239W-EGFP expression (Fig. 6b).

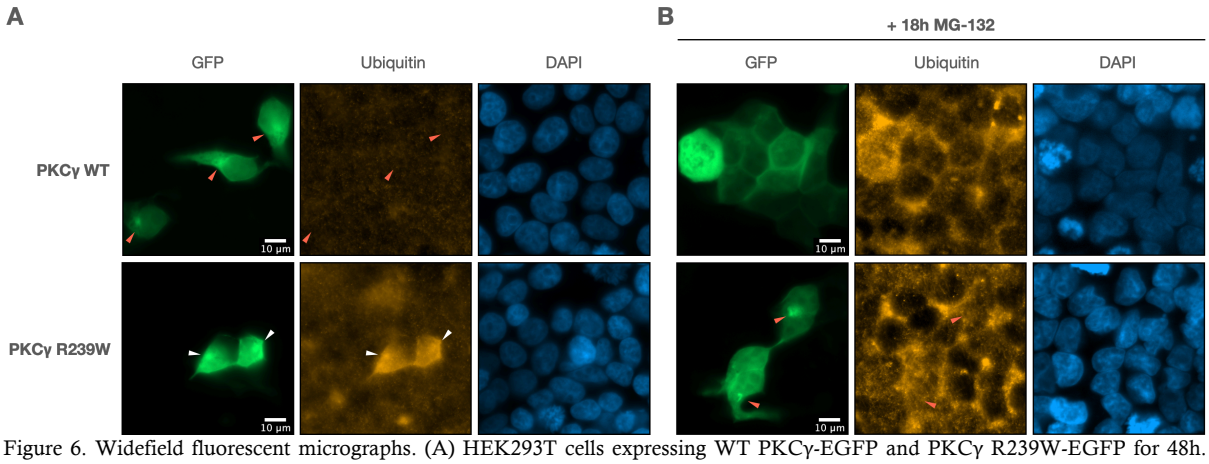

Figure 6. Widefield fluorescent micrographs. (A) HEK293T cells expressing WT PKCγ-EGFP and PKCγ R239W-EGFP for 48h. (B) HEK293T cells expressing WT PKCγ-EGFP and PKCγ R239W-EGFP for 48h and treated with 10 µM MG132 for 18h. Immunocytochemistry was performed with specific antibodies to detect ubiquitin and visualized with Cy3-conjugated secondary antibodies (n = 2). Representative images shown. Scale bar denotes 10 µm.

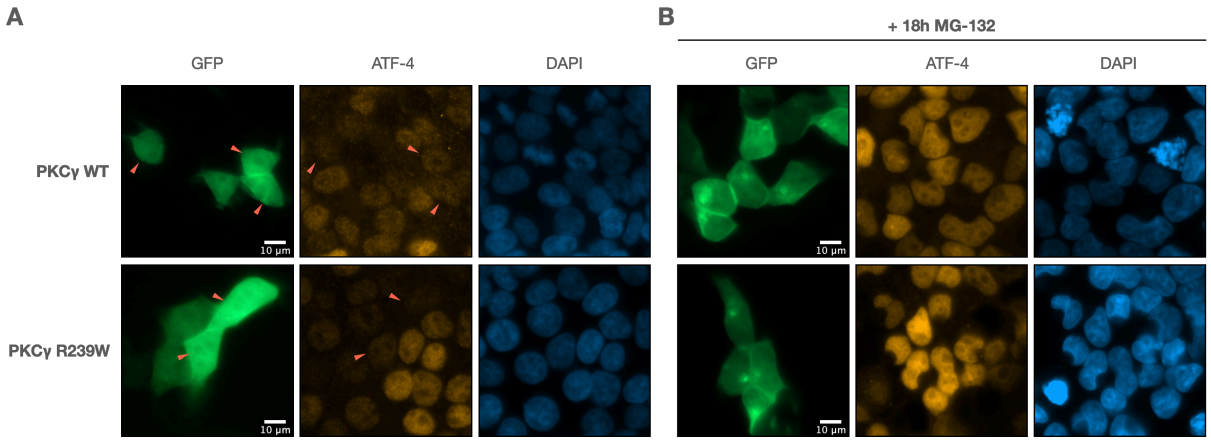

Figure 7. Widefield fluorescent micrographs. (A) HEK293T cells expressing WT PKCγ-EGFP and PKCγ R239W-EGFP for 48h. (B) HEK293T cells expressing WT PKCγ-EGFP and PKCγ R239W-EGFP for 48h and treated with 10 µM MG132 for 18h. Immunocytochemistry was performed with specific antibodies to detect ATF-4 and visualized with Cy3-conjugated secondary antibodies (n = 2). Representative images shown. Scale bar denotes 10 µm.

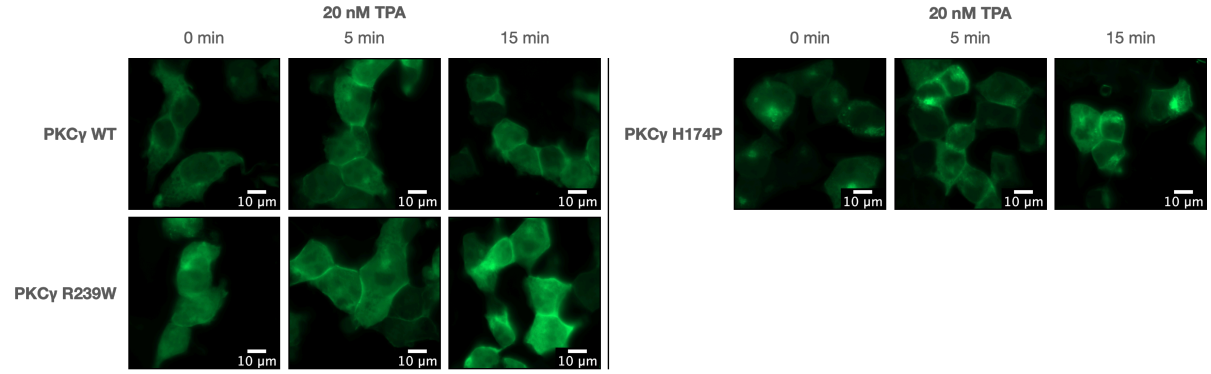

Figure 8. Widefield fluorescent micrographs of HEK293T cells expressing WT PKCγ-EGFP, PKCγ R239W-EGFP, and PKCγ H174P-EGFP for 48h and stimulated with 20 nM TPA for 0, 5, and 15 minutes before fixating and mounting (n = 2). Representative images shown. Scale bar denotes 10 µm.

PKCγ R239W does not cause ER stress

We also explored whether the impaired degradation of PKCγ R239W-EGFP induced the unfolded protein response (UPR) of the endoplasmic reticulum (ER). To this end, we transiently expressed WT PKCγ-EGFP and PKCγ R239W-EGFP for 48h in HEK293T cells and performed immunofluorescence against ATF-4, a transcription factor that is upregulated and localizes to the nucleus upon ER-stress (Pitale et al., 2017). As a positive control, one half was subjected to 18h treatment with 10 µM proteasome inhibitor MG-132 before fixating. For cells expressing WT PKCγ-EGFP and PKCγ R239W-EGFP, we observed varying intensities of ATF-4 that localized to nuclei but could not correlate this to the expression of either PKCγ (Fig. 7a). In cells treated with proteasome inhibitor MG-132, we observed an increase in nuclear-localized ATF-4 in all cells but could not correlate this to the expression of PKCγ-EGFP WT or R239W (Fig. 7b).

PKCγ R239W and H174P translocate upon stimulation with TPA

In the past, phorbol ester-induced plasma membrane translocation of PKCγ has been shown to be impaired by pathogenic PKCγ mutations (Seki et al., 2005; Verbeek et al., 2008). To study whether the R239W and H174P variants also impaired PKCγ translocation, we transiently expressed WT PKCγ-EGFP, PKCγ R239W-EGFP, and PKCγ H174P-EGFP in HEK293T cells for 48h. In the past, others have used 400 nM 12-O-tetradecanoylphorbol-13-acetate (TPA) to study PKCγ translocation (Seki et al., 2005; Verbeek et al., 2008), but we observed high toxicity upon using this concentration. We observed that 20 nM TPA is sufficient to induce WT PKCγ-EGFP translocation to the plasma membrane within 5 minutes (Fig. 8). Similarly, we observed mild translocation of PKCγ R239W-EGFP and PKCγ H174P-EGFP upon 5 minutes of stimulation with 20 nM TPA (Fig. 8). However, PKCγ R239W-EGFP and PKCγ H174P-EGFP in foci did not translocate.

PKCγ R239W translocates upon stimulation with Ca2+ ionophore A23187

Others have shown in the past that, besides stimulation of the C1 domain with TPA, PKCγ translocation can also be induced upon stimulation of the C2 domain with calcium ionophore A23187 (Sakai et al., 1997;

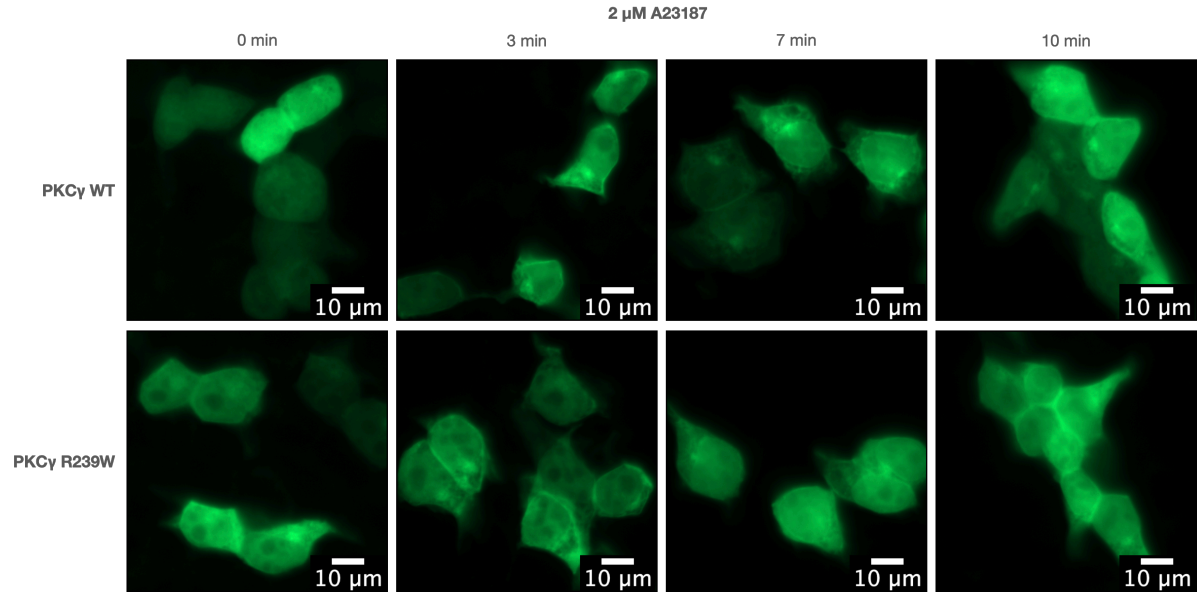

Figure 9. Widefield fluorescent micrographs of HEK293T cells expressing WT PKCγ-EGFP and PKCγ R239W-EGFP for 48h and stimulated with 2 µM A23187 for 0, 3, 7 and 10 minutes before fixating and mounting (n = 2). Representative images shown. Scale bar denotes 10 µm.

Verbeek et al., 2005). It has been shown that some pathogenic PKCγ mutations affect the translocation of PKCγ upon C2 domain stimulation (Sakai et al., 1997; Verbeek et al., 2005).

To study whether the R239W and H174P variants also impaired Ca^{++}-induced PKCγ translocation, we transiently transfected HEK293T cells with WT PKCγ-EGFP, PKCγ R239W-EGFP, and PKCγ H174P-EGFP and stimulated cells with A23187 48h post-transfection to study the translocation with fluorescent microscopy.

Previously, 80 µM A23187 was used to study PKCγ translocation (Sakai et al., 1997). However, we observed high toxicity using this concentration (data not shown). After optimizing, we observed that 2 µM A23187 is sufficient to induce WT PKCγ-EGFP translocation to the plasma membrane within 3 minutes (Fig. 9). Similarly, we observed mild translocation of PKCγ R239W-EGFP upon 3 minutes of stimulation with 2 µM A23187 (Fig. 9). Unfortunately, the transfection for PKCγ H174P-EGFP failed in this experiment, and therefore we were unable to perform this translocation experiment.

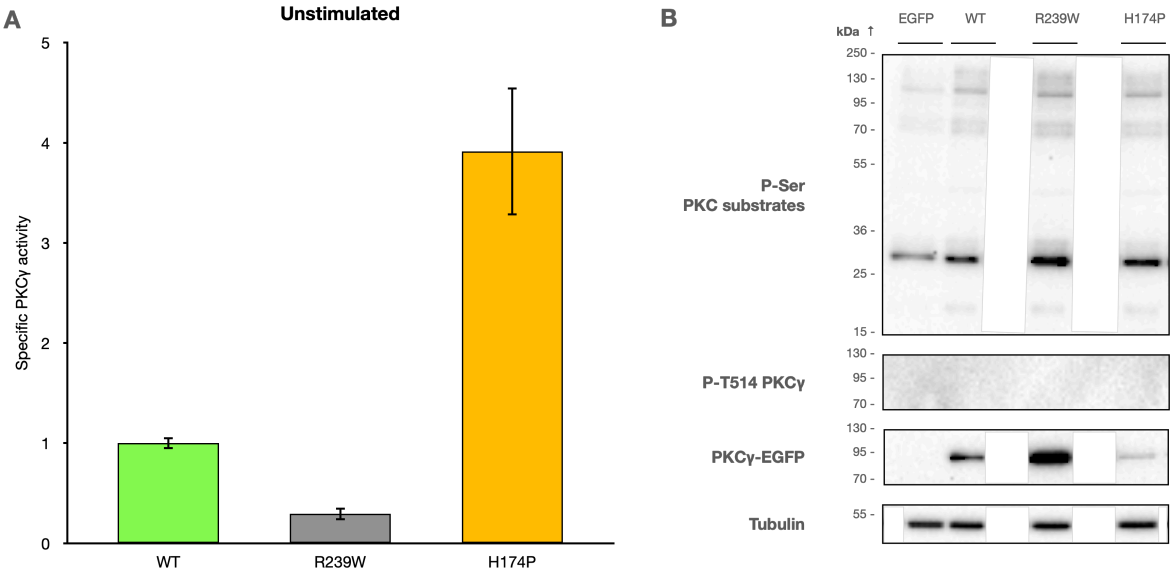

Figure 10. (A) Relative kinase activity, quantified as the phosphorylation of PKC substrates normalized to tubulin and GFP, in HEK293T cells expressing WT PKCγ-EGFP, PKCγ R239W-EGFP, and PKCγ H174P-EGFP for 48h (n = 3). Bars represent mean ± standard deviation (n = 3).
(B) Immunoblot of EGFP, WT PKCγ-EGFP, PKCγ R239W-EGFP, and PKCγ H174P-EGFP. Lysates from transiently transfected HEK293T cells were run on 10% gels under denaturing conditions. After transfer to PVDF membrane the blotted bands were immunodetected with specific antibodies against P-Ser PKC substrates, P-T514 PKCγ, GFP, and tubulin, and subsequently visualized with peroxidase labeled secondary antibodies. Images are from nonconsecutive wells on the same blot.

H174P and R239W variants affect basal PKCγ kinase activity

To study if the R239W and H174P variants affect PKCγ kinase activity, we transiently expressed EGFP, WT PKCγ-EGFP, PKCγ R239W-EGFP, and PKCγ H174P for 48h in HEK293T cells. First, we sought to study the autophosphorylation of PKCγ as a measure of intrinsic kinase activity by immunoblotting against phosphorylated Thr514 (P-T514) (Jezierska et al., 2014; Wong et al., 2018). Unfortunately, we failed to detect any phosphorylated T514-PKCγ, either endogenous or overexpressed (Fig. 10b).

Next, we investigated the phosphorylation status of serine residues (P-Ser) of PKC substrates mediated by endogenous PKCγ and by overexpressed PKCγ-WT-EGFP, PKCγ-R239W-EGFP, and PKCγ-H174P-EGFP. Relative phosphorylation of the downstream targets was quantified as described in the Methods section.

The data in Figure 10b showed an increase in phosphorylated PKC substrates upon overexpression of either variant or wildtype. We observed no difference between the level of phosphorylated PKC substrates in cells expressing the variants R239W and H174P compared to wildtype PKCγ.

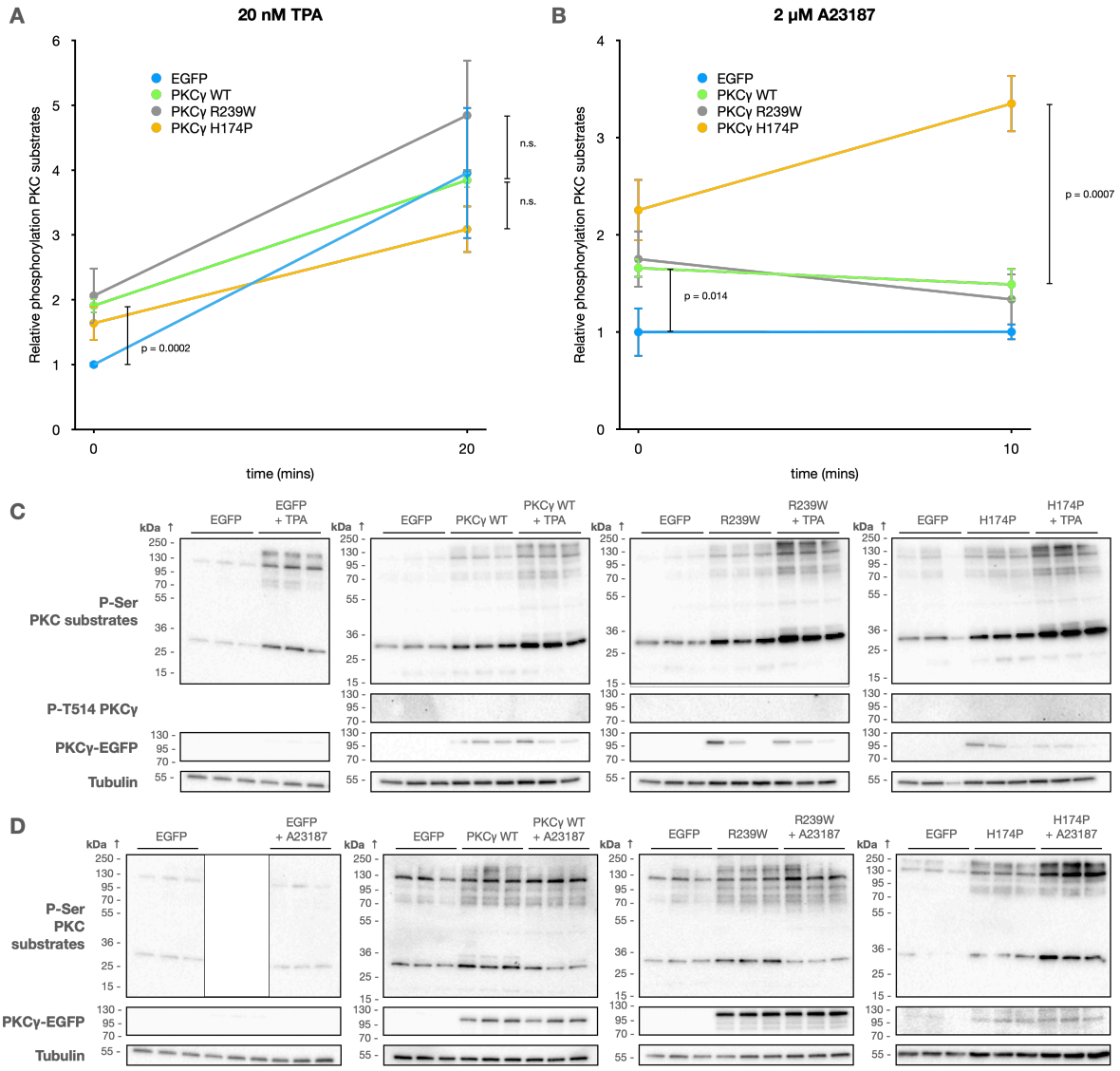

Figure 11. (A) Relative phosphorylation of PKC substrates normalized to tubulin, in HEK293T cells expressing EGFP, WT PKCγ-EGFP, PKCγ R239W-EGFP, and PKCγ H174P-EGFP for 48h, and stimulated with 20 nM TPA for 0 and 20 mins (n = 3). Graphs represent mean ± standard deviation (n = 3). Significant differences (unpaired Student t-test, two-tailed) are indicated with their p-values.
(B) Relative phosphorylation of PKC substrates normalized to tubulin, in HEK293T cells expressing EGFP, WT PKCγ-EGFP, PKCγ R239W-EGFP, and PKCγ H174P-EGFP for 48h, and stimulated with 2 µM A23187 for 0 and 10 mins (n = 3).
(C) Immunoblot of EGFP, WT PKCγ-EGFP, PKCγ R239W-EGFP, and PKCγ H174P-EGFP stimulated with 20 nM TPA for 0 and 20 mins. After transfer to PVDF membrane the blotted bands were immunodetected with specific antibodies against P-Ser PKC substrates, P-T514 PKCγ, GFP, and tubulin, and subsequently visualized with peroxidase labeled secondary antibodies.
(D) Immunoblot of EGFP, WT PKCγ-EGFP, PKCγ R239W-EGFP, and PKCγ H174P-EGFP stimulated with 2 µM A23187 for 0 and 10 mins. Blotted bands were immunodetected with specific antibodies against P-Ser PKC substrates, PKCγ, and tubulin.

However, when normalizing the level of phosphorylated PKC substrates to the protein abundance of overexpressed PKCγ, we observed that the H174P variant increased the basal activity of PKCγ and that R239W decreased the basal activity, as reflected by the phosphorylation level of the PKC substrates (Fig. 10a).

PKCγ is activated by TPA stimulation

Following up, we studied whether the variants in the C2 domain affected the TPA-induced kinase activity of PKCγ by assessing the increase in phosphorylated PKC substrates over time. To this end, we transiently expressed EGFP, WT PKCγ-EGFP, PKCγ R239W-EGFP, and PKCγ H174P-EGFP for 48h in HEK293T cells and stimulated with 20 nM TPA for 20 mins, before performing immunoblotting.

Immunoblot analysis showed an increase in the levels of phosphorylated PKC substrates upon 20 mins of TPA stimulation in EGFP-expressing cells and in cells overexpressing PKCγ-WT-EGFP, PKCγ-R239W-EGFP, and PKCγ-H174P-EGFP (Fig. 11c). However, we did not see a significant difference in phosphorylated PKC substrates upon stimulation between endogenous PKCγ, overexpressed PKCγ-WT-EGFP, PKCγ-R239W-EGFP, and PKCγ-H174P-EGFP (Fig. 11a).

PKCγ H174P is activated by calcium ionophore stimulation

Since WT PKCγ-EGFP and PKCγ R239W-EGFP translocated upon stimulation with calcium ionophore A23187, we next studied the effects of this stimulation on the phosphorylation of PKC substrates by WT PKCγ-EGFP, PKCγ R239W-EGFP, and PKCγ H174P-EGFP with immunoblotting.

To study the effect of calcium ionophore A23187 stimulation on the kinase activity of different variants, transiently expressed EGFP, PKCγ-WT-EGFP, PKCγ-R239W-EGFP, and PKCγ-H174P-EGFP for 48h in HEK293T cells. We again used 2μM A23187 to study the downstream phosphorylation of PKC substrates by the different variants. However, this time we stimulated the overexpressing cells for 10 mins before performing immunoblotting.

As can be seen in Figures 11b and 11d, stimulation with calcium ionophore A23187 did not increase the phosphorylation of PKC substrates in EGFP-, WT PKCγ-EGFP-, or PKCγ R239W-EGFP-expressing cells. Interestingly, we did observe a significant increase in P-Ser of PKC substrates upon stimulation with A23187 in cells expressing PKCγ H174P-EGFP (Fig. 11b).

Creating an isogenic disease model in neuron-like cells

Besides studying the effects of the R239W and H174P variants on PKCγ using overexpression, we sought to develop a cell model that is more physiologically relevant. Instead of HEK293T cells, we made use of the human neuroblastoma cell line SH-SY5Y and introduced the R239W and H174P variants through the novel CRISPR technique prime editing (PE), to explore what the functional effects of these missense variants would be when introduced in endogenous PKCγ (Anzalone et al., 2019).

The SH-SY5Y cell line was chosen since it can be differentiated into a neuronal-like cell type expressing PKCγ, making it a popular human cell line for studying neurodegenerative diseases (Kovalevich & Langford, 2013; Murillo et al., 2017; Pezzini et al., 2017). It is a mostly diploid cell line (Yusuf et al., 2013), which makes it preferential for genomic editing. Moreover, because SH-SY5Y is a human cell line, the findings would be more translatable to the disease than when done in a cell line from other organisms.

In the present study, we made use of the prime editing systems PE2 and PE3B to introduce the R239W and H174P variants in *PRKCG* in SH-SY5Y cells as described in the Methods section. We transiently transfected SH-SY5Y cells with either PE2 or PE3B plasmids targeting the R239W edit and with PE2 plasmids targeting the H174P edit.

Three days post-transfection, we observed expression of the pCMV-PE2-P2A-GFP plasmid using live-cell fluorescent microscopy. We continued culturing the cells to ensure that prime editing had taken place.

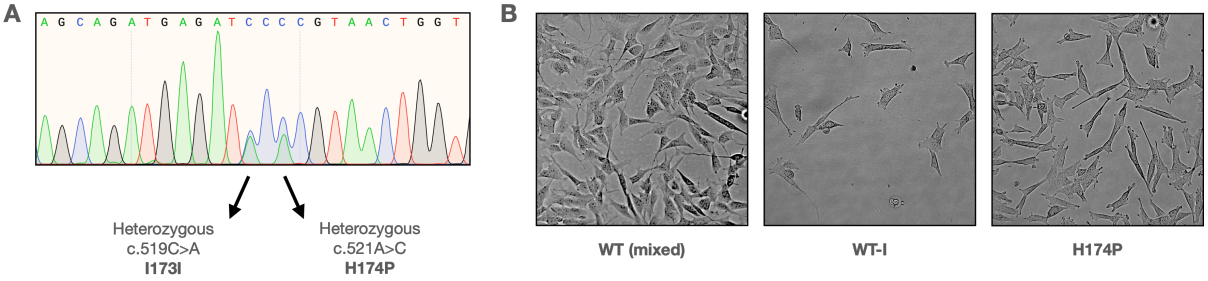

Figure 12. (A) Sequencing chromatogram of heterozygous PKCγ H174P SH-SY5Y clone. Mutations were validated with Sanger sequencing. The PAM sequence mutation c.519C>A was introduced to prevent nicking of the edited DNA strand.
(B) Brightfield live cell micrographs of WT (mixed), WT-I, and heterozygous PKCγ H174P SH-SY5Y cells in culture.

After five days of culturing, fluorescence activated cell sorting was performed to sort single GFP-expressing

and propidium iodide-negative cells into 96-well culture plates. In this way, 192 clones were sorted expressing the R239W PE2 system, 192 clones expressing the R239W PE3B system, and 192 clones expressing the H174P PE2 system.

After applying the prime editing CRISPR/Cas9 technique and screening 53 of 192 clones, we successfully obtained an SH-SY5Y clone heterozygous for the H174P variant (Fig. 12a). In parallel, after screening 61 of 192 PE2 clones and 47 of 192 PE3B clones, no clone was identified with the R239W variant.

Morphology

When culturing the heterozygous H174P cell line, we observed that its morphology was different from the wildtype cell line from which it was derived (Fig. 12b). Since the SH-SY5Y cell line consists of a heterogeneous population, we compared the heterozygous H174P cell line to single-cell sorted subclones of wildtype SH-SY5Y cells and found that its morphology closely resembles the intermediate phenotype (WT-I; Fig. 12b).

PKCγ expression

Next, we sought to investigate the functional effect of the H174P variant on PKCγ. Since PKCγ is only expressed in SH-SY5Y cells after differentiation, we first stimulated heterozygous H174P cells, WT-I cells, and WT (mixed) cells with 10 µM ATRA for five days to induce differentiation, followed by treatment with 50 ng/ml BDNF to promote proliferation.

After three days of stimulation with 10 µM ATRA, using brightfield microscopy, we observed increased cell death in the heterozygous H174P cells compared to WT-I and WT cells. We continued the differentiation protocol for 18 days total, and observed cell death in H174P cells up to the 12th day of culturing (Fig. 13). As can be seen in Figure 13c, the stimulation with ATRA causes a decrease in cell confluency in both heterozygous H174P cells and WT-I cells. However, the decrease in cell confluency from day 3 to day 8 was greater in heterozygous H174P cells than in WT-I cells.

To investigate if the observed toxicity was caused by induced expression of PKCγ, the heterozygous H174P cells, WT-I, and WT cells were lysed on day 0, day 5, and day 18 of the differentiation protocol to perform immunoblotting. First, immunoblotting was performed against PKCγ, using a polyclonal antibody with affinity against WT PKCγ as well as PKCγ H174P. Second, to study if the endogenous expression of PKCγ H174P caused changes in the phosphorylation profile, immunoblotting was performed against P-Ser of PKC substrates. Third, to study whether differentiation was induced in heterozygous H174P cells,

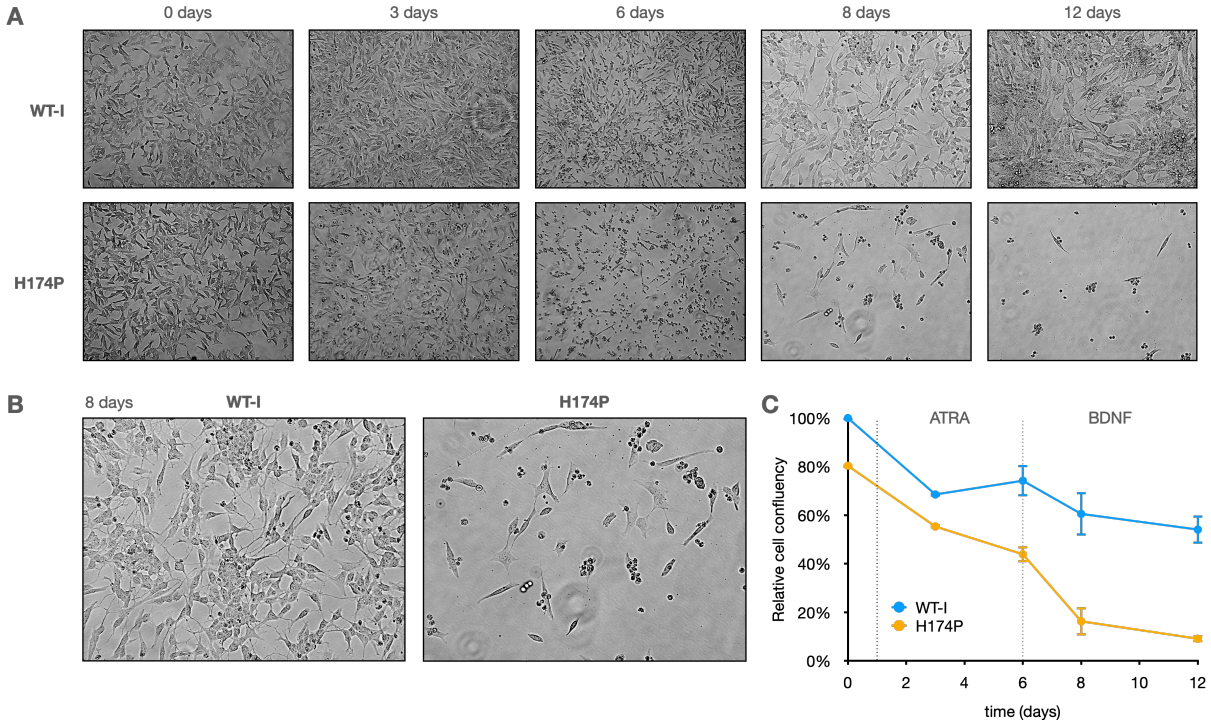

Figure 13. (A) Brightfield live cell micrographs of WT-I and heterozygous PKCγ H174P SH-SY5Y cells upon induction of differentiation. From day 1 to day 6, cells were stimulated with 10 µM ATRA. From day 6 to day 18, cells were stimulated with 50 ng/ml BDNF.
(B) Enlarged micrographs of WT-I and heterozygous PKCγ H174P SH-SY5Y on day 8 of differentiation.
(C) Cell confluency upon induction of differentiation as quantified by image analysis on brightfield micrographs. Graphs represent mean ± standard deviation (day 0 and day 3: n = 1; day 6 and day 8: n = 5; day 12: n = 6).

immunoblotting was performed against tyrosine hydroxylase. Lastly, immunoblotting was performed against tubulin. Unfortunately, immunoblotting failed for all targets (Fig. 14).

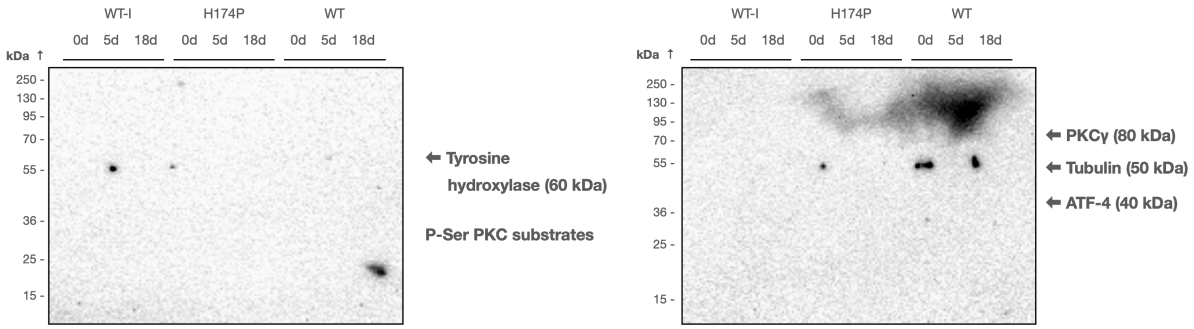

Figure 14. Immunoblots of WT-I, heterozygous PKCγ H174P, and WT (mixed) SH-SY5Y cells on day 0, day 5, and day 18 of differentiation. Lysates were run on 10% gels under denaturing conditions. After transfer to PVDF membrane the blotted bands were immunodetected with specific antibodies against tyrosine hydroxylase, P-Ser PKC substrates, PKCγ, ATF-4, and tubulin, and subsequently visualized with peroxidase labeled secondary antibodies.

Discussion

To reclassify the SCA14 VUSes H174P and R239W, we performed functional studies using overexpression models in HEK293T cells, as well as an isogenic SH-SY5Y cell model heterozygous for the PKCγ H174P variant.

PKCγ H174P and R239W form aggregates

In the present study, we have shown that the H174P and R239W variants caused PKCγ to form cytoplasmic condensates upon overexpression (Fig. 2). However, we noticed that the PKCγ H174P and R239W aggregates were different in morphology (Fig. 3a). Our data showed that PKCγ R239W primarily formed aggregates with a massive appearance and localized to the concave part of the nucleus, which is thought to be the aggresome (Fig. 3b). Contrastingly, we noticed that PKCγ H174P was more prone to aggregate and predominantly formed foci with a dot-like appearance (Fig. 3b). We investigated whether the different aggregate morphology was caused by changes in protein degradation. Previously, it had been shown that pathogenic PKCγ mutations in the C1 domain caused the formation of similar aggregates (Seki et al., 2005, 2007; Wong et al., 2018). These aggregates first appeared as dot-like foci but progressed into massive aggregates upon sequestering proteasomes, thereby impairing their own degradation and causing ER stress and subsequent apoptosis (Seki et al., 2007).

Our data suggest that the PKCγ R239W aggregates are formed similarly. We have shown that PKCγ R239W was highly ubiquitinated and therefore targeted for degradation (Fig. 6a). However, we found that PKCγ R239W accumulated more than WT PKCγ at steady-state and was not degraded upon inhibition of protein synthesis (Fig. 4a, 5a), indicating that R239W inhibits proteasomal PKCγ degradation. It remains elusive how PKCγ R239W evades degradation, causing accumulation and aggregation. One explanation is that PKCγ R239W aggregates might sequester proteasomes, as was previously shown to occur for other C1 domain mutants (Seki et al., 2007). Another possible explanation could be that PKCγ R239W cannot be dephosphorylated, which has been shown to impair proteasomal degradation of mutant PKCγ (Jezierska et al., 2014; Wong et al., 2018). Future experiments need to be done to elucidate through which mechanism PKCγ R239W resists degradation.

Although the overexpression of PKCγ R239W caused it to form aggregates and impaired its own proteasomal degradation, we found that it did not cause an increase in nuclear-localized ATF-4 (Fig. 7a), suggesting that PKCγ R239W did not elicit the ER-UPR. This was surprising since the induction of ER stress is a hallmark of many protein misfolding diseases and has been reported for pathogenic C1 domain mutants (Lindholm et al., 2006; Seki et al., 2007). The finding that PKCγ R239W did not cause ER stress does not necessarily mean that the aggregates are benign. On the contrary, the misfolding of proteins often exposes hydrophobic regions that normally compose the inside of the protein. This can result in the toxic gain-of-function of the protein through nonspecific interactions with other proteins, sequestering them into the aggregates that PKCγ R239W forms. These toxic protein aggregates are an important hallmark for many neurodegenerative diseases (Sabath et al., 2020). We therefore suggest that PKCγ R239W similarly causes pathogenesis through aggregation and the loss of proteostasis. This could be followed up on by performing long-term live-cell microscopy to study if the expression of PKCγ R239W and the formation of its aggregates causes cell death.

Contrary to most reported pathogenic PKCγ mutants, PKCγ H174P aggregates occurred mainly in the dot-like configuration, and the coagulation into massive aggregates was seemingly prevented (Fig. 2, 3a). Previously, some pathogenic PKCγ mutations have been reported that similarly form dot-like foci, although they progressed more often into massive aggregates (Seki et al., 2007). It is therefore interesting how the coagulation of PKCγ aggregates is prevented by the H174P variant. Although we did not study the degradation kinetics of PKCγ H174P upon inhibition of protein synthesis, we did observe that PKCγ H174P was much less abundant than WT PKCγ (Fig. 4). We presume that the lower abundance of PKCγ H174P is caused by rapid turn-over of the protein due to its high propensity to misfold. In turn, this degradation would prevent the progression from dot-like foci to massive aggregates. Others have shown that the clearance of dot-like PKCγ aggregates, but not massive aggregates, was dependent on autophagy (Yamamoto et al., 2010). Additional experiments should be performed to study the degradation kinetics and whether the dot-like PKCγ H174P aggregates could progress into massive aggregates.

The H174P and R239W variants affect PKCγ activity

Besides causing protein aggregation, we investigated whether the H174P and R239W variants affected the kinase activity of PKCγ. Increased or dysregulated PKC activity is associated with neurodegeneration in Alzheimer's disease and SCA (Newton, 2018). Many missense mutations in the C1 domain have been reported to increase the kinase activity and cause pathogenesis through this gain of function mechanism (Jezierska et al., 2014; Wong et al., 2018). Because the H174P and R239W variants are in the regulatory C2

domain, and we have previously shown that these variants cause conformational changes that destabilize the protein, we hypothesized that these variants would increase the activity of PKCγ.

Since we could not measure the phosphorylation of PKCγ at T514 as a readout for its intrinsic activity (Fig. 10b), we chose to study its activity by measuring the relative phosphorylation of its downstream targets. We found that the overexpression of PKCγ WT, PKCγ R239W, and PKCγ H174P all increased the phosphorylation of PKC substrates compared to cells overexpressing EGFP (Fig. 10b). However, when normalizing the increase in downstream phosphorylation to the different protein levels of the respective overexpressed PKCγ, we found that the H174P variant increased the basal activity of PKCγ (Fig. 10a). Taken together with our previous finding that PKCγ H174P was conformationally unstable and formed aggregates, we suggest that this unstable conformation prevented interactions between the kinase domain and its pseudo-substrate domain. As such, the H174P variant has lost an essential regulatory mechanism, leading to a gain of function in PKCγ.

Conversely, we found that the R239W variant decreased the basal activity of PKCγ (Fig. 10a). Others have shown that pathogenic mutants of PKCγ affected the phosphorylation of PKCγ, causing decreased kinase activity as well as accumulation of PKCγ in aggregates (Adachi et al., 2008; Jezierska et al., 2014; Verbeek et al., 2008). However, the loss of function in kinase activity has not been associated directly with neurodegeneration (Newton, 2018). Instead, others have reported that the pathogenicity of loss of function mutations in PKCγ is caused by the formation of aggregates that induce ER stress (Seki et al., 2005, 2007). However, as previously mentioned, we did not find proof that PKCγ R239W induced ER stress.

Moreover, it was shown that the loss of function variants in the C1 domain had reduced kinase activity upon TPA stimulation (Verbeek et al., 2008). Upon investigation, we observed that the R239W and H174P variants did not impair the translocation of PKCγ to the plasma membrane after stimulation with TPA (Fig. 8). Moreover, we have shown that PKCγ R239W translocated to the plasma membrane upon stimulation with a calcium ionophore, similar to WT PKCγ (Fig. 9). Therefore, the R239W and H174P variants did not affect the affinity of the C1 domain for TPA, and the R239W variant did not affect the affinity of the C2 domain for Ca^{++} (Fig. 9). As such, we suggest that the R239W variant does not affect ligand binding in either domain. Instead, we presume that the loss of function in PKCγ R239W is caused by increased interactions between the kinase domain and the pseudo-substrate domain.

Although we had observed that the R239W and H174P variants caused differences in basal PKCγ activity (Fig. 10a), we found no significant difference in the phosphorylation of downstream targets upon TPA stimulation (Fig. 11a). The equal increase upon stimulation could be explained by the saturated phosphorylation of substrates by the activity of endogenous PKCs. Further analysis needs to be performed to confirm this, by taking a measurement at an earlier time point, by studying the TPA-stimulated kinase activity *in vitro*, or by studying the phosphorylation of downstream targets in an isogenic cell model.

Despite the observation that stimulation with a calcium ionophore was sufficient to translocate PKCγ WT and PKCγ R239W to the plasma membrane (Fig. 9), we found that it is not sufficient for PKCγ WT and PKCγ R239W to become enzymatically active (Fig. 11b). This suggests that PKCγ WT and PKCγ R239W require (co-)stimulation with DAG (TPA) to become enzymatically active. This is in line with the current model for conventional PKCs, as the binding of Ca^{++} increases the affinity towards DAG. The binding of DAG at the plasma membrane is required and sufficient to release the pseudo-substrate from the kinase domain, upon which the latter becomes active (Newton, 2010).

Ca^{++} signaling is sufficient to activate PKCγ H174P

PKCγ H174P was not present at the plasma membrane without stimulation (Fig. 8). However, we did measure an increased basal kinase activity by measuring the phosphorylation of downstream targets (Fig. 10). Based on this, we previously suggested that the conformational change caused by the H174P variant prevented interactions between the kinase domain and its pseudo-substrate domain. Moreover, we found that kinase activity (i.e. the phosphorylation of downstream targets) was increased exclusively in PKCγ H174P upon Ca^{++} stimulation. Taken together, we suggest that the H174P variant has lost the requirement for DAG (TPA) to activate PKCγ (Fig. 11b). As such, any increase in intracellular Ca^{++} is sufficient to activate PKCγ H174P, causing phosphorylation of downstream targets. This is in agreement with the increased basal activity of PKCγ H174P, since Ca^{++} is always present in the cell. Moreover, this further supports the hypothesis that the H174P variant has dysregulated PKCγ activity, which has been shown to cause pathology in SCA14 (Ji et al., 2014; Newton, 2018; Verbeek et al., 2005).

In an isogenic cell model of heterozygous PKCγ H174P SH-SY5Y cells, we have shown that the induction of differentiation and, therefore, the expression of PKCγ H174P (Korecka et al., 2013; Murillo et al., 2017) caused toxicity (Fig. 13c). Unfortunately, we could not study this biochemically (Fig. 14). However, based on overexpression experiments, we reported that the H174P variant caused a gain of function in PKCγ through elevated basal activity and an additional increase in activity upon Ca^{++} stimulation. This gain of function mechanism caused dysregulation of the phosphorylation profile of the

cells (Fig. 10a, 11b). It has been shown that ATRA-induced differentiation of SH-SY5Y cells causes remodeling of calcium stores, thereby increasing intracellular Ca^{++} levels, which was sufficient to activate PKCγ H174P (Bell et al., 2013; Newton, 2010; Pieri et al., 1997; Wu et al., 2003). Dysregulation of Ca^{++} signaling has been shown to be the cause of various other SCAs and other neurodegenerative diseases (Kasumu & Bezprozvanny, 2012). Therefore, we suggest that the ATRA-induced toxicity in H174P SH-SY5Y cells was caused by the combination of increased basal activity of PKCγ H174P and increased intracellular Ca^{++} concentration upon differentiation that further increased the activity of PKCγ H174P. In transgene mice models of SCA14, increased and dysregulated PKC activity caused Purkinje cell dysfunction with impaired neurite growth and a marked ataxia (Shimobayashi & Kapfhammer, 2021).

A different explanation lies in the aggregation we reported before. We have shown that the H174P variant readily misfolds upon overexpression and forms cytoplasmic dot-like foci. Others have shown that similar aggregates formed by other pathogenic PKCγ mutants caused apoptosis through ER-stress (Seki et al., 2007). It is possible that the expression of PKCγ H174P caused apoptosis in SH-SY5Y cells through a similar mechanism. This is unlikely, however, since we did not observe any toxicity in HEK293T cells overexpressing PKCγ H174P.

The extreme toxicity that we observed in upon differentiation of the H174P cells was unexpected from the perspective of the disease since SCA14 is a late-onset type of ataxia. One would expect the phenotype we reported in cell lines to translate to a very early onset of the disease in patients since Purkinje cells are expanded and differentiated in the first year of life (Miyata et al., 1999).

The possibility exists that the toxicity that we observed upon differentiation is not caused by the H174P variant, but by off-target mutations introduced by the genome editing. Although the originators had developed the prime editing technique to minimize the probability of introducing off-target edits (Anzalone et al., 2019), it is not impossible that off-target edits occurred in the creation of the heterozygous PKCγ H174P clone. The presence of such off-target events could be investigated by sequencing genomic regions that share similarities to the intended edit site. However, in the present study, we did not confirm the absence of off-target mutations in the heterozygous H174P clone that was created, as the pegRNAs and sgRNAs controlling the genomic edit were designed carefully, and the predicted probability of introducing off-target mutations was minimized accordingly. Although we cannot fully exclude the possibility of introducing off-target mutations, and while we do suggest that this should be assessed, we conclude that the observed toxicity upon inducing differentiating the heterozygous PKCγ H174P clone was definitely a phenotype of the H174P variant, as it was in line with the dysregulated biological activity of overexpressed PKCγ H174P.

Conclusion

We conclude that PKCγ R239W causes pathogenesis through impairing proteasomal degradation, which leads to the accumulation of PKCγ and the formation of toxic protein aggregates. Contrary to our hypothesis that the R239W variant would increase PKCγ activity, we found that the basal activity of PKCγ R239W is, in fact, decreased compared to WT PKCγ, suggesting a loss of function.

Furthermore, we conclude that PKCγ H174P also causes pathogenesis through the formation of protein aggregates, as well as dysregulated kinase activity which spontaneously phosphorylates its downstream targets. It is logical that this dysregulated kinase activity caused the cytotoxicity that was observed upon differentiating the heterozygous PKCγ H174P SH-SY5Y mutant.

As such, we suggest reclassifying the current VUS R239W as likely-pathogenic since it needs more support, although it shares many features with other pathogenic PKCγ mutants. We also strongly suggest reclassifying the current VUS H174P as pathogenic since we have shown through multiple mechanisms and in different cell models that the H174P mutation leads to a toxic gain of function of PKCγ.

Acknowledgments

I would like to kindly thank Dineke Verbeek for giving me the opportunity to do my internship and project in her lab, for providing the required facilities, and for professional guidance on the project. I would also like to thank Michiel Fokkens for his guidance on performing CRISPR/Cas9 Prime editing technique, cloning of Prime editing constructs, and screening the clones for mutations. My grateful thanks are also extended to Kai Yu Ma, for assisting in troubleshooting the SH-SY5Y differentiation experiment and for supplying us with the SH-SY5Y WT-I clone, to Miriam Langelaar-Makkinje of the Department of Pediatrics, for assistance with fluorescent microscopy and for providing various chemicals, to Michel Meijer of the Department of Biomedical Sciences of Cells and Systems, for supplying us with the SH-SY5Y cell line, and to Geert Mesander and Theo Bijma of the Flow Cytometry Unit, for their assistance on performing the flow cytometry experiments.

References

Adachi, N., Kobayashi, T., Takahashi, H., Kawasaki, T., Shirai, Y., Ueyama, T., Matsuda, T., Seki, T., Sakai, N., & Saito, N. (2008). Enzymological Analysis of Mutant Protein Kinase Cγ Causing Spinocerebellar Ataxia Type 14 and Dysfunction in Ca2+ Homeostasis. *Journal of Biological Chemistry*, *283*(28), 19854–19863. https://doi.org/10.1074/jbc.M801492200

Anzalone, A. V., Randolph, P. B., Davis, J. R., Sousa, A. A., Koblan, L. W., Levy, J. M., Chen, P. J., Wilson, C., Newby, G. A., Raguram, A., & Liu, D. R. (2019). Search-and-replace genome editing without double-strand breaks or donor DNA. *Nature*, *576*(7785), 149–157. https://doi.org/10.1038/s41586-019-1711-4

Bell, N., Hann, V., Redfern, C. P. F., & Cheek, T. R. (2013). Store-operated Ca2+ entry in proliferating and retinoic acid-differentiated N- and S-type neuroblastoma cells. *Biochimica et Biophysica Acta - Molecular Cell Research*, *1833*(3), 643–651. https://doi.org/10.1016/j.bbamcr.2012.11.025

Carlson, K. M., Andresen, J. M., & Orr, H. T. (2009). Emerging pathogenic pathways in the spinocerebellar ataxias. *Current Opinion in Genetics and Development*, *19*(3), 247–253. https://doi.org/10.1016/j.gde.2009.02.009

Chen, D. H., Brkanac, Z., Verlinde, C. L. M. J., Tan, X. J., Bylenok, L., Nochlin, D., Matsushita, M., Lipe, H., Wolff, J., Fernandez, M., Cimino, P. J., Bird, T. D., & Raskind, W. H. (2003). Missense mutations in the regulatory domain of PKCγ: A new mechanism for dominant nonepisodic cerebellar ataxia. *American Journal of Human Genetics*, *72*(4), 839–849. https://doi.org/10.1086/373883

Chow, R. D., & Chen, S. (2020). pegFinder: A pegRNA designer for CRISPR prime editing. *BioRxiv*, *3825*, 2020.05.06.081612. https://www.biorxiv.org/content/10.1101/2020.05.06.081612v1%0Ahttps://www.biorxiv.org/content/10.1101/2020.05.06.081612v1.abstract

Deneault, E., Chaineau, M., Nicouleau, M., Castellanos Montiel, M. J., Franco Flores, A. K., Haghi, G., Chen, C. X. Q., Abdian, N., Shlaifer, I., Beitel, L. K., & Durcan, T. M. (2021). A streamlined CRISPR workflow to introduce mutations and generate isogenic iPSCs for modeling amyotrophic lateral sclerosis. *Methods*. https://doi.org/10.1016/j.ymeth.2021.09.002

Ellard, S., Baple, E. L., Callaway, A., Berry, I., Forrester, N., Turnbull, C., Owens, M., Eccles, D. M., Abbs, S., Scott, R., Deans, Z. C., Lester, T., Campbell, J., Newman, W. G., Ramsden, S., & McMullan, D. J. (2020). ACGS Best Practice Guidelines for Variant Classification in Rare Disease 2020. *Association for Clinical Genomic Science*, 531210.

Ghorbani, F., Alimohamed, M. Z., Vilacha, J. F., Van Dijk, K. K., De Boer-Bergsma, J., Fokkens, M. R., Lemmink, H., Sijmons, R. H., Sikkema-Raddatz, B., Groves, M. R., Verschuuren-Bemelmans, C. C., Verbeek, D. S., Van Diemen, C. C., & Westers, H. (2022). Feasibility of Follow-Up Studies and Reclassification in Spinocerebellar Ataxia Gene Variants of Unknown Significance. *Frontiers in Genetics*, *13*(March), 1–13. https://doi.org/10.3389/fgene.2022.782685

Jezierska, J., Goedhart, J., Kampinga, H. H., Reits, E. A., & Verbeek, D. S. (2014). SCA14 mutation V138E leads to partly unfolded PKCγ associated with an exposed C-terminus, altered kinetics, phosphorylation and enhanced insolubilization. *Journal of Neurochemistry*, *128*(5), 741–751. https://doi.org/10.1111/jnc.12491

Ji, J., Hassler, M. L., Shimobayashi, E., Paka, N., Streit, R., & Kapfhammer, J. P. (2014). Increased protein kinase C gamma activity induces Purkinje cell pathology in a mouse model of spinocerebellar ataxia 14. *Neurobiology of Disease*, *70*, 1–11. https://doi.org/10.1016/j.nbd.2014.06.002

Jumper, J., Evans, R., Pritzel, A., Green, T., Figurnov, M., Ronneberger, O., Tunyasuvunakool, K., Bates, R., □ídek, A., Potapenko, A., Bridgland, A., Meyer, C., Kohl, S. A. A., Ballard, A. J., Cowie, A., Romera-Paredes, B., Nikolov, S., Jain, R., Adler, J., … Hassabis, D. (2021). Highly accurate protein structure prediction with AlphaFold. *Nature*, *596*(7873), 583–589. https://doi.org/10.1038/s41586-021-03819-2

Kasumu, A., & Bezprozvanny, I. (2012). Deranged Calcium Signaling in Purkinje Cells and Pathogenesis in Spinocerebellar Ataxia 2 (SCA2) and Other Ataxias. *The Cerebellum*, *11*(3), 630–639. https://doi.org/10.1007/s12311-010-0182-9

Kim, H. K., Yu, G., Park, J., Min, S., Lee, S., Yoon, S., & Kim, H. H. (2021). Predicting the efficiency of prime editing guide RNAs in human cells. *Nature Biotechnology*, *39*(2), 198–206. https://doi.org/10.1038/s41587-020-0677-y

Korecka, J. A., van Kesteren, R. E., Blaas, E., Spitzer, S. O., Kamstra, J. H., Smit, A. B., Swaab, D. F., Verhaagen, J., & Bossers, K. (2013). Phenotypic Characterization of Retinoic Acid Differentiated SH-SY5Y Cells by Transcriptional Profiling. *PLoS ONE*, *8*(5).

https://doi.org/10.1371/journal.pone.0063862
Kovalevich, J., & Langford, D. (2013). Considerations for the Use of SH-SY5Y Neuroblastoma Cells in Neurobiology. In S. Amini & M. K. White (Eds.), *Neuronal Cell Culture: Methods and Protocols* (Vol. 1078, pp. 9–21). Humana Press. https://doi.org/10.1007/978-1-62703-640-5_2
Lee, D. H., & Goldberg, A. L. (1996). Selective inhibitors of the proteasome-dependent and vacuolar pathways of protein degradation in Saccharomyces cerevisiae. *Journal of Biological Chemistry*, *271*(44), 27280–27284. https://doi.org/10.1074/jbc.271.44.27280
Li, S.-C., Goto, N. K., Williams, K. A., Deber, C. M., & Fasman, G. D. (1996). Sheet, Propensity of Proline Is Determined By Peptide Environment. *Biochemistry A-Helical*, *93*(June), 6676–6681.
Lindholm, D., Wootz, H., & Korhonen, L. (2006). ER stress and neurodegenerative diseases. *Cell Death and Differentiation*, *13*(3), 385–392. https://doi.org/10.1038/sj.cdd.4401778
Miyata, M., Miyata, H., Mikoshiba, K., & Ohama, E. (1999). Development of Purkinje cells in humans: an immunohistochemical study using a monoclonal antibody against the inositol 1, 4, 5-triphosphate type 1 receptor (IP3R1). *Acta Neuropathologica*, *98*(3), 226–232. https://doi.org/10.1007/s004010051073
Murillo, J. R., Goto-Silva, L., Sánchez, A., Nogueira, F. C. S., Domont, G. B., & Junqueira, M. (2017). Quantitative proteomic analysis identifies proteins and pathways related to neuronal development in differentiated SH-SY5Y neuroblastoma cells. *EuPA Open Proteomics*, *16*(November 2016), 1–11. https://doi.org/10.1016/j.euprot.2017.06.001
Newton, A. C. (2010). Protein kinase C: poised to signal. *American Journal of Physiology-Endocrinology and Metabolism*, *298*(3), E395–E402. https://doi.org/10.1152/ajpendo.00477.2009
Newton, A. C. (2018). Protein kinase C: perfectly balanced. *Critical Reviews in Biochemistry and Molecular Biology*, *53*(2), 208–230. https://doi.org/10.1080/10409238.2018.1442408
Pezzini, F., Bettinetti, L., Di Leva, F., Bianchi, M., Zoratti, E., Carrozzo, R., Santorelli, F. M., Delledonne, M., Lalowski, M., & Simonati, A. (2017). Transcriptomic Profiling Discloses Molecular and Cellular Events Related to Neuronal Differentiation in SH-SY5Y Neuroblastoma Cells. *Cellular and Molecular Neurobiology*, *37*(4), 665–682. https://doi.org/10.1007/s10571-016-0403-y
Pieri, A., Liguri, G., Ceechi, C., Degl'Innocenti, D., Nassi, P., & Ramponi, G. (1997). Alteration of intracellular free calcium and acylphosphatase levels in differentiating SH-SY5Y neuroblastoma cells. *IUBMB Life*, *43*(3), 633–641. https://doi.org/10.1080/15216549700204441
Pitale, P. M., Gorbatyuk, O., & Gorbatyuk, M. (2017). Neurodegeneration: Keeping ATF4 on a tight leash. *Frontiers in Cellular Neuroscience*, *11*(December), 1–8. https://doi.org/10.3389/fncel.2017.00410
Prelich, G. (2012). Gene overexpression: Uses, mechanisms, and interpretation. *Genetics*, *190*(3), 841–854. https://doi.org/10.1534/genetics.111.136911
Sabath, N., Levy-Adam, F., Younis, A., Rozales, K., Meller, A., Hadar, S., Soueid-Baumgarten, S., & Shalgi, R. (2020). Cellular proteostasis decline in human senescence. *Proceedings of the National Academy of Sciences of the United States of America*, *117*(50), 31902–31913. https://doi.org/10.1073/pnas.2018138117
Sakai, N., Sasaki, K., Ikegaki, N., Shirai, Y., Ono, Y., & Saito, N. (1997). Direct visualization of the translocation of the γ-subspecies of protein kinase C in living cells using fusion proteins with green fluorescent protein. *Journal of Cell Biology*, *139*(6), 1465–1476. https://doi.org/10.1083/jcb.139.6.1465
Schmitz-Hübsch, T., Lux, S., Bauer, P., Brandt, A. U., Schlapakow, E., Greschus, S., Scheel, M., Gärtner, H., Kirlangic, M. E., Gras, V., Timmann, D., Synofzik, M., Giorgetti, A., Carloni, P., Shah, J. N., Schöls, L., Kopp, U., Bußenius, L., Oberwahrenbrock, T., … Minnerop, M. (2021). Spinocerebellar ataxia type 14: refining clinicogenetic diagnosis in a rare adult-onset disorder. *Annals of Clinical and Translational Neurology*, *8*(4), 774–789. https://doi.org/10.1002/acn3.51315
Seki, T., Adachi, N., Ono, Y., Mochizuki, H., Hiramoto, K., Amano, T., Matsubayashi, H., Matsumoto, M., Kawakami, H., Saito, N., & Sakai, N. (2005). Mutant protein kinase Cγ found in spinocerebellar ataxia type 14 is susceptible to aggregation and causes cell death. *Journal of Biological Chemistry*, *280*(32), 29096–29106. https://doi.org/10.1074/jbc.M501716200
Seki, T., Takahashi, H., Adachi, N., Abe, N., Shimahara, T., Saito, N., & Sakai, N. (2007). Aggregate formation of mutant protein kinase C gamma found in spinocerebellar ataxia type 14 impairs ubiquitin-proteasome system and induces endoplasmic reticulum stress. *European Journal of Neuroscience*, *26*(11), 3126–3140. https://doi.org/10.1111/j.1460-9568.2007.05933.x
Shimobayashi, E., & Kapfhammer, J. P. (2017). Increased biological activity of protein Kinase C gamma is not required in Spinocerebellar ataxia 14. *Molecular Brain*, *10*(1), 34. https://doi.org/10.1186/s13041-017-0313-z
Shimobayashi, E., & Kapfhammer, J. P. (2021). A New Mouse Model Related to SCA14 Carrying a

Pseudosubstrate Domain Mutation in PKCγ Shows Perturbed Purkinje Cell Maturation and Ataxic Motor Behavior. *The Journal of Neuroscience*, *41*(9), 2053–2068. https://doi.org/10.1523/JNEUROSCI.1946-20.2021

Soong, B. W., & Paulson, H. L. (2007). Spinocerebellar ataxias: An update. *Current Opinion in Neurology*, *20*(4), 438–446. https://doi.org/10.1097/WCO.0b013e3281fbd3dd

van Gaalen, J., Vermeer, S., van Veluw, M., Van de Warrenburg, B. P. C., & Dooijes, D. (2013). A de novo SCA14 mutation in an isolated case of late-onset cerebellar ataxia. *Movement Disorders*, *28*(13), 1902–1903. https://doi.org/10.1002/mds.25572

Verbeek, D. S., Goedhart, J., Bruinsma, L., Sinke, R. J., & Reits, E. A. (2008). PKCγ mutations in spinocerebellar ataxia type 14 affect C1 domain accessibility and kinase activity leading to aberrant MAPK signaling. *Journal of Cell Science*, *121*(14), 2339–2349. https://doi.org/10.1242/jcs.027698

Verbeek, D. S., Knight, M. A., Harmison, G. G., Fischbeck, K. H., & Howell, B. W. (2005). Protein kinase C gamma mutations in spinocerebellar ataxia 14 increase kinase activity and alter membrane targeting. *Brain*, *128*(2), 436–442. https://doi.org/10.1093/brain/awh378

Wong, M. M. K., Hoekstra, S. D., Vowles, J., Watson, L. M., Fuller, G., Németh, A. H., Cowley, S. A., Ansorge, O., Talbot, K., & Becker, E. B. E. (2018). Neurodegeneration in SCA14 is associated with increased PKCγ kinase activity, mislocalization and aggregation. *Acta Neuropathologica Communications*, *6*(1), 99. https://doi.org/10.1186/s40478-018-0600-7

Wu, J., Tan, X., Peng, X., Yuan, J., & Qiang, B. (2003). Translocation and Phosphorylation of Calcyclin Binding Protein during Retinoic Acid-induced Neuronal Differentiation of Neuroblastoma SH-SY5Y Cells. *BMB Reports*, *36*(4), 354–358. https://doi.org/10.5483/BMBRep.2003.36.4.354

Yamamoto, K., Seki, T., Adachi, N., Takahashi, T., Tanaka, S., Hide, I., Saito, N., & Sakai, N. (2010). Mutant protein kinase C gamma that causes spinocerebellar ataxia type 14 (SCA14) is selectively degraded by autophagy. *Genes to Cells*, *15*(5), 425–438. https://doi.org/10.1111/j.1365-2443.2010.01395.x

Yusuf, M., Leung, K., Morris, K. J., & Volpi, E. V. (2013). Comprehensive cytogenomic profile of the in vitro neuronal model SH-SY5Y. *Neurogenetics*, *14*(1), 63–70. https://doi.org/10.1007/s10048-012-0350-9

Supplementary Materials

Supplementary Table 1. Oligonucleotides used for mutagenesis PCR, cloning of pegRNAs and sgRNA, and Surveyor PCR.

Mutagenesis primers	**Sequence (5' – 3')**
pEGFP-N1 PKCγ H174P sense	CAGATGAGATCCCCGTAACTGTTGGC
pEGFP-N1 PKCγ H174P antisense	GCCAACAGTTACGGGGATCTCATCTG
gRNA inserts	
pegRNA PKCγ R239W sense	caccgCCCACACCTCCACGCTGAGCGTTTTAGA GCTAGAAATAGCAAGTTAAAATAAGGCTAGT CCGTTATCAACTTGAAAAAGTGGCACCGAGT CGGTGCTGGAGCGCTGGCTCAGCGTGGAG
pegRNA PKCγ R239W antisense	aaaaCTCCACGCTGAGCCAGCGCTCCAGCACC GACTCGGTGCCACTTTTTCAAGTTGATAACG GACTAGCCTTATTTTAACTTGCTATTTCTAGC TCTAAAACGCTCAGCGTGGAGGTGTGc
pegRNA PKCγ H174P sense	caccGCGGGGCCTCACCAGTTACGGTTTTAGA GCTAGAAATAGCAAGTTAAAATAAGGCTAGT CCGTTATCAACTTGAAAAAGTGGCACCGAGT CGGTGCATGAGATACCCGTAACTGGTGAGGC
pegRNA PKCγ H174P antisense	aaaaGCCTCACCAGTTACGGGTATCTCATGCAC CGACTCGGTGCCACTTTTTCAAGTTGATAACG GACTAGCCTTATTTTAACTTGCTATTTCTAGC TCTAAAACCGTAACTGGTGAGGCCCCGC
sgRNA PE3B PKCγ R239W sense	caccgTGTGGAGCGCTGGCTCAGCG
sgRNA PE3B PKCγ R239W antisense	aaacCGCTGAGCCAGCGCTCCACAc
Surveyor PCR primers	
PKCγ R239W sense	CGGAGAGACAGCCAGACCACTG
PKCγ R239W antisense	GTGCGCATGCTGGGAGGCAGAGG
PKCγ H174P sense	CAAGTTCCGCCTGCATAGCTACAG
PKCγ H174P antisense	GAGCAACAAGAGCGAAACTCCGTC

Supplementary Table 2. Antibodies used for immunoblotting and immunocytochemistry.

Antibodies for immunoblotting			
Primary antibodies	**Clonality**	**Dilution**	**Supplier**
Mouse-anti-actin	Monoclonal	1:10,000	MP Biochemicals #8691001
Mouse anti-Living colors	Monoclonal	1:5,000	ClonTech #632381 JL-8
Mouse anti-PKC66	Monoclonal	1:1,000	Invitrogen #13-3800
Mouse anti-tubulin	Monoclonal	1:10,000	Sigma
Rabbit anti-PKCγ	Polyclonal	1:1,000	Santa Cruz sc-211
Rabbit anti-P-Ser PKC substrates	Polyclonal	1:1,000	Cell Signaling Technology #9379
Rabbit anti-tyrosine hydroxylase	Polyclonal	1:1,000	Millipore Sigma AB152
Secondary antibodies			
Goat-anti-mouse IgG (H+L) HRP-conjugated	Polyclonal	1:10,000	Bio-Rad #170-6516
Goat-anti-rabbit IgG (H+L) HRP-conjugated	Polyclonal	1:10,000	Bio-Rad #170-6515
Antibodies for immunofluorescence			
Primary antibodies			
Mouse anti-ubiquitin	Monoclonal	1:100	Cell Signaling Technology #3936 P4D1
Rabbit anti-ATF-4	Monoclonal	1:200	Cell Signaling Technology #11815 D4B8
Secondary antibodies			
Donkey-anti-mouse IgG (H+L) Cy3-conjugated	Polyclonal	1:250	Jackson ImmunoResearch #715-165-150
Donkey-anti-rabbit IgG (H+L) Cy3-conjugated	Polyclonal	1:250	Jackson ImmunoResearch #711-165-152